Scaling of longitudinal and transverse velocity increments in a cylinder wake

T. Zhou,* Z. Hao, L. P. Chua, and S. C. M. Yu
School of Mechanical and Aerospace Engineering, Nanyang Technological University, Singapore 639798
(Received 20 January 2005; published 21 June 2005)

Longitudinal and transverse velocity increments are measured both temporally and spatially using two X-wire probes in the intermediate region of a cylinder wake over Taylor microscale Reynolds numbers in the range of 100–300. The scaling exponents of both the spatial and temporal longitudinal velocity increments agree favorably with the predictions of Kolmogorov and She and Leveque. The scaling exponents of the transverse velocity increments are considerably smaller than those of the longitudinal ones, with the values for spatial transverse velocity increments being slightly larger than the temporal ones. The difference between the scaling exponents of the longitudinal and transverse velocity increments is examined against the refined similarity hypotheses for transverse velocity increments (RSHT) proposed by Chen *et al.* It is found that the RSHT can account for the difference between the scaling exponents of the longitudinal and spatial transverse velocity increments at all Reynolds numbers considered.

DOI: 10.1103/PhysRevE.71.066307 PACS number(s): 47.27.Ak

I. INTRODUCTION

The similarity hypotheses proposed by Kolmogorov [1] (hereafter K41) and the later revision (Kolmogorov [2] or K62) are crucially important in the study of small-scale turbulence. The main assumptions used in these hypotheses are the local isotropy and very large Reynolds numbers both in the dissipative range (DR) ($r \ll L$, where L is the integral length scale of turbulence) and in the inertial range (IR) ($\eta \ll r \ll L$, where $\eta \equiv \nu^{3/4}/\langle\varepsilon\rangle^{1/4}$ is the Kolmogorov length scale, $\langle\varepsilon\rangle$ and ν are the mean energy dissipation rate and kinematic viscosity, respectively, and the angular brackets denote time averaging). According to K41,

$$\langle(\delta\alpha)^n\rangle \sim (r\langle\varepsilon\rangle)^{n/3}, \tag{1}$$

when r is in the inertial range, where $\delta\alpha \equiv \alpha(x+r)-\alpha(x)$ is the velocity increment. In the definition of $\delta\alpha$, α represents any component (u, v, or w) of the velocity fluctuations in the longitudinal (streamwise), transverse, and spanwise directions, respectively, and r is the separation between the two points. If the velocity component is in the same direction as the separation of the two points, it is defined as a longitudinal one. In contrast, if the velocity component is perpendicular to the separation r, $\delta\alpha$ is referred to as the transverse velocity increment.

Over the past years, extensive experimental and numerical investigations have highlighted that the scaling exponents of $\langle(\delta\alpha)^n\rangle$ deviate from $n/3$, known as the anomalous scaling. This anomalous scaling is normally attributed to the so-called small-scale intermittency. To account for the spatial and temporal intermittency effect of the energy dissipative rate, Kolmogorov [2] introduced the refined similarity hypothesis (RSH). One consequence in K62 is that the moments of the velocity increments $\langle(\delta\alpha)^n\rangle$ scale as

$$\langle(\delta\alpha)^n\rangle \sim r^{\zeta_\alpha(n)} \tag{2}$$

in the IR, where $\zeta_\alpha(n)$ are the scaling exponents of $\langle(\delta\alpha)^n\rangle$ and may not be equal to $n/3$.

The K62, or indeed K41 hypotheses, did not distinguish between nth-order moments of the longitudinal velocity increment δS_L and the transverse velocity increment δS_T. The most common method to measure δS_L is temporally sampling the velocity fluctuations u along the main flow direction. Taylor's hypothesis is used to convert the temporal delay τ to a spatial increment r in the streamwise direction: i.e.,

$$\delta S_{L,1} = \delta u(r) = u(x+r) - u(x), \tag{3}$$

with $r \equiv \tau U$, where U is the local mean velocity in the streamwise direction. Note that the subscript number "1" next to L has been used here to distinguish $\delta S_{L,1}$ from that introduced later.

Several methods can be used to determine δS_T. One way is to sample the transverse velocity component v or w using an X-wire probe at a fixed location of the flow. δS_T can then be obtained using

$$\delta S_{T,1} = w(x+r) - w(r) \ [\text{or } v(x+r) - v(r)]. \tag{4}$$

Taylor's hypothesis is again used to convert the temporal delay to a spatial separation r. The subscript number next to T distinguishes between different definitions for δS_T used here. Another definition of δS_T is the spatial transverse velocity increment, defined as

$$\delta S_{T,2} \equiv u(z+\Delta z) - u(z), \tag{5}$$

where z is in the spanwise direction. An important advantage of this definition is that the influence of the large-scale velocity anisotropy is removed from the scaling of $\langle(\delta S_{T,2})^n\rangle$. With only a few exceptions [3–5], recent experiments [6–10] and direct numerical simulation (DNS) [11,12] have shown that the scaling exponents $\zeta_T(n)$, associated with the moments of δS_T—viz., $\langle(\delta S_T)^n\rangle \sim r^{\zeta_T(n)}$—are slightly smaller than those of δS_L, where $\langle(\delta S_L)^n\rangle \sim r^{\zeta_L(n)}$. Other experiments

*Electronic address: mtmzhou@ntu.edu.sg

[13–16] have shown that $\zeta_T(n)$ are significantly smaller than $\zeta_L(n)$. Extensive studies have been conducted to explain the differences between $\zeta_T(n)$ and $\zeta_L(n)$. Possible explanations include (1) the anisotropy of the flow (e.g., [9,16–23]), (2) the effect of Reynolds number (e.g., [15,16,24–27]), (3) the effect of the initial and boundary conditions [23,28], and (4) the intermittencies affecting the longitudinal and transverse velocity structure functions [11,14]. It needs to be noted that the above explanations may not necessarily unrelated. Boratav and Pelz [14] suggested that the difference between $\zeta_T(n)$ and $\zeta_L(n)$ is the result of the different contributions from the strain-dominated structures and the enstrophy-dominated structures to the longitudinal and transverse velocity increments. Chen *et al.* [11] proposed and verified numerically a modified model to the RSH, which they called the refined similarity hypothesis for transverse velocity increments (RSHT). The RSHT has been tested by Antonia *et al.* [13] and Zhou and Antonia [15] in decaying grid turbulence. These authors found that the RSHT can only partially account for the difference of the scaling exponents between the longitudinal and transverse velocity increments. They suggested that the anisotropy of turbulence structures in the scaling range, which reflects the small values of R_λ in their study, is more likely to account for most of the difference, where R_λ is the Taylor microscale Reynolds number defined as $R_\lambda = \langle u' \rangle \lambda / \nu$ [$\lambda \equiv u' / (\partial u / \partial x)'$ is the longitudinal Taylor microscale, a superscript prime represents the root-mean-square (rms) values]. It needs to be noted that in the study of Antonia *et al.* [13] and Zhou and Antonia [15], δS_T was obtained from the measurements of v using an X-wire probe [i.e., Eq. (4)]. The RSHT was verified satisfactorily by Bi and Wei [10], where δS_T was obtained using both an X-wire probe and a rake of single hot wires. The significant difference between the scaling exponents of the longitudinal and transverse velocity increments was also explained [7,8,16] by the different definitions used to obtain δS_T and the method for estimating $\zeta_T(n)$, especially for shear flows with small and moderate values of R_λ.

Recently, significant attention has been given to the extraction of anisotropic contributions from velocity structure functions using both experiments (e.g., [17,18,20]) and numerical simulations [19,21,22]. The approach is based on the so-called decomposition of the velocity correlations or structure functions in terms of the irreducible representation of the SO(3) group of spatial rotation in three dimensions [19,29]. The isotropic sector of this decomposition is the zeroth-order term which can be disentangled from the anisotropic part [18]. The intension of this decomposition is to assess the persistence of anisotropic effects on inertial as well as the dissipative scales.

More recently, Romano and Antonia [23] proposed a model to account for the effect of the large-scale anisotropy in the far field of the round jets. The effect of the large-scale anisotropy is assessed by considering the different initial conditions at the jet nozzle and hence different ratios of the longitudinal and transverse rms velocities. This model explains reasonably well the difference in the scaling exponents between longitudinal and transverse velocity structure functions in plane wakes generated by various bluff bodies [9].

In the present study, we aim to investigate the scaling exponents of the longitudinal and transverse velocity increments measured both temporally and spatially and their dependence on the Reynolds number on the centerline of turbulent wakes using data obtained from two X-wire probes. The longitudinal velocity increment δS_L is obtained using both Eq. (3) and the following relation:

$$\delta S_{L,2} = \delta w(r) = w(z + \Delta z) - w(z). \tag{6}$$

The transverse velocity increment δS_T is obtained using Eqs. (4) and (5). The transverse vorticity component is also measured, allowing a direct check of the RSHT at different Reynolds numbers.

II. EXPERIMENTAL DETAILS

The experiments were conducted in a closed-loop wind tunnel with dimensions of 1.2 m (width) $\times$ 0.8 m (height) and 2.2 m long. Velocity fluctuations u and w at the downstream location of 75d were measured using two X-wire probes aligned on the centerline of the wake generated by a circular cylinder with a diameter d of 25.4 mm. The cylinder was located vertically 20 cm downstream of the entrance of the test section. The two X-wire probes were aligned in the x-z plane so that u and w can be measured simultaneously. The coordinate system, the cylinder, and the arrangement of the two X-wire probes are shown in Fig. 1. The upper X-wire probe is attached to a traversing mechanism and is able to move along the spanwise direction so as to achieve the desired separation (Δz) while the lower X-wire probe was kept stable 20 cm above the bottom wall of the tunnel. The flow conditions of the free stream have been checked to be uniform in the wind tunnel with turbulent intensity less than 0.5%. The measurements were conducted under four free-stream velocities: i.e., 5 m/s, 10 m/s, 15 m/s, and 20 m/s, corresponding to R_λ of 100, 200, 250, and 300, respectively. The transverse vorticity component ω_y can be approximated by

$$\omega_y = \frac{\partial u}{\partial z} - \frac{\partial w}{\partial x} \approx \frac{\Delta u}{\Delta z} - \frac{\Delta w}{\Delta x}, \tag{7}$$

where Δu is the difference between u from the two X-wires; Δw is the difference between values of w at the same point in space, but separated in time by two sampling time intervals (where central difference is used). Because the turbulence intensity is relatively small ($u'/U \leqslant 10\%$), the use of Taylor's hypothesis—i.e., $\Delta / \Delta x = -U^{-1} \Delta / \Delta t$—in Eq. (7) should be satisfactory.

The hot wires were operated with in-house constant-temperature circuits at an over heat ratio of 1.5. Each of the two wires had a diameter of 2.5 μm. The wire separation was about 1 mm. The output signals were low-pass filtered through the buck and gain circuits at the cutoff frequencies $f_c = 1.6$ kHz, 5.2 kHz, 9.2 kHz, and 9.2 kHz, respectively, for the four free-stream velocities, which are close to the Kolmogorov frequency $f_K = U_1 / 2\pi\eta$ except at the highest R_λ. The filtered signals were sampled at a frequency $f_s = 2 f_c$ into a PC using a 16-bit analog-to-digital (A/D) converter (Na-

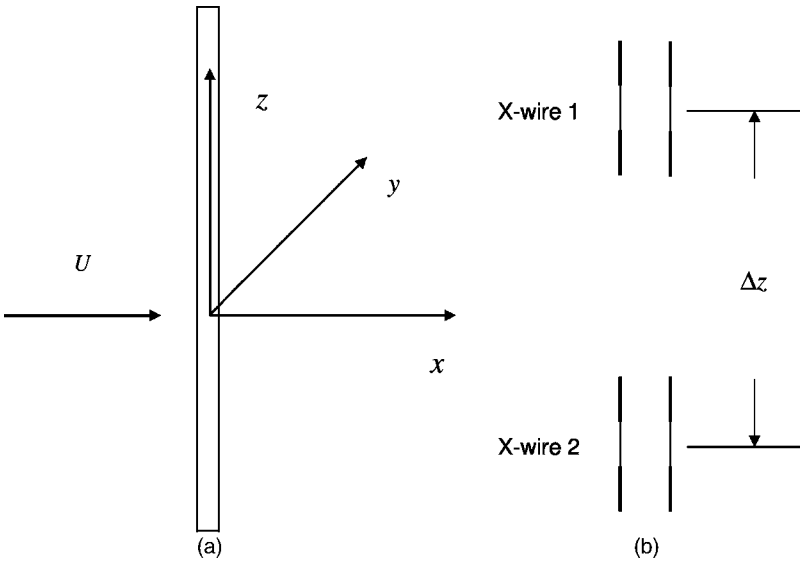

FIG. 1. Coordinate system and probe arrangement. (a) Coordinate system and (b) probe arrangement (front view).

tional Instrument). The sampling period was 120 s for all velocities. Further analysis of the data was done using the MATLAB programs.

III. RELATIONSHIP BETWEEN THE SECOND-ORDER LONGITUDINAL AND TRANSVERSE VELOCITY INCREMENTS

For isotropic turbulence, the second-order longitudinal and transverse velocity increments are related [30] via

$$\langle(\delta S_T)^2\rangle_{\rm iso} = \left(1 + \frac{r}{2}\frac{d}{dr}\right)\langle(\delta S_L)^2\rangle. \tag{8}$$

The subscript "iso" means that the values of $\langle(\delta S_T)^2\rangle$ are calculated from Eq. (8) using the measured values of $\langle(\delta S_L)^2\rangle$. The calculated values of $\langle(\delta S_T^*)^2\rangle_{\rm iso}$ are compared with $\langle(\delta S_{T,1}^*)^2\rangle$ and $\langle(\delta S_{T,2}^*)^2\rangle$ in Fig. 2. (Note that only results for $R_\lambda = 250$ are shown here. The same level of agreement can be found for other values of Reynolds numbers.) Hereafter, an asterisk represents quantities normalized by the Kolmogorov length scale η and/or velocity scale u_K ($\equiv \nu/\eta$). The distribution of $\langle(\delta S_{L,1}^*)^2\rangle$ agrees favorably with that of $\langle(\delta S_{L,2}^*)^2\rangle$ over the range of $20 \leqslant r^* \leqslant 500$. For scales $r^* < 20$, the departure of $\langle(\delta S_{L,2}^*)^2\rangle$ from $\langle(\delta S_{L,1}^*)^2\rangle$ may be caused by the noise effect of the probes. The errors in measuring the initial separation between the two X-wire probes may not be completely dismissed. For large scales, the departure may be caused by the global anisotropy, which is reflected by the ratio $w'/u' \approx 0.85$ (note that for global isotropy, the ratio is equal to 1). There exists good agreement between $\langle(\delta S_T^*)^2\rangle_{\rm iso}$ and $\langle(\delta S_{T,2}^*)^2\rangle$ for $r^* < 300$, verifying local isotropy in this region. The agreement between $\langle(\delta S_T^*)^2\rangle_{\rm iso}$ and $\langle(\delta S_{T,1}^*)^2\rangle$ is poor except over a very narrow region ($r^* < 50$). The results shown in Fig. 2 seem to suggest that local isotropy [Eq. (8)] is better satisfied by the spatial transverse velocity increments than the temporal ones in low- to moderate-Reynolds-number flows. For the longitudinal velocity increments, there is always satisfactory agreement between spatial and temporal methods.

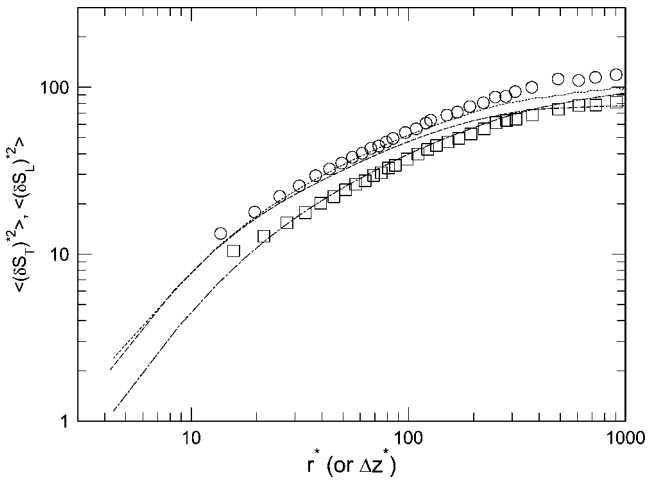

FIG. 2. Comparison of measured second-order transverse structure functions with isotropic calculation [Eq. (8)]: dot-dashed line, $\langle(\delta S_{L,1}^*)^2\rangle$; □, $\langle(\delta S_{L,2}^*)^2\rangle$; long-dashed line, $\langle(\delta S_{T,1}^*)^2\rangle$; ○, $\langle(\delta S_{T,2}^*)^2\rangle$; short-dashed line, $\langle(\delta S_T^*)^2\rangle_{\rm iso}$.

IV. SCALING EXPONENTS OF THE LONGITUDINAL AND TRANSVERSE VELOCITY INCREMENTS

In the present study, due to the limited values of R_λ, an apparent inertial range, over which $\langle(\delta S_L^{*3})\rangle$ depends linearly on r^*, cannot be defined unambiguously even at $R_\lambda = 300$. To estimate the scaling exponents of the velocity increments, the extended self-similarity (ESS) method [31] is used with a slight modification—the region where $\langle|\delta S_L|^3\rangle$ is approximately linear to r is used to define the scaling range (SR). This method has been widely used for estimating the scaling exponents (e.g., [7,9,20,32]). The corresponding scaling exponents are known as the values relative to the third-order velocity increments. Distributions of $\langle|\delta S_L^*|^3\rangle r^{*-1}$ for different values of R_λ are shown in Fig. 3. There exist apparent scaling

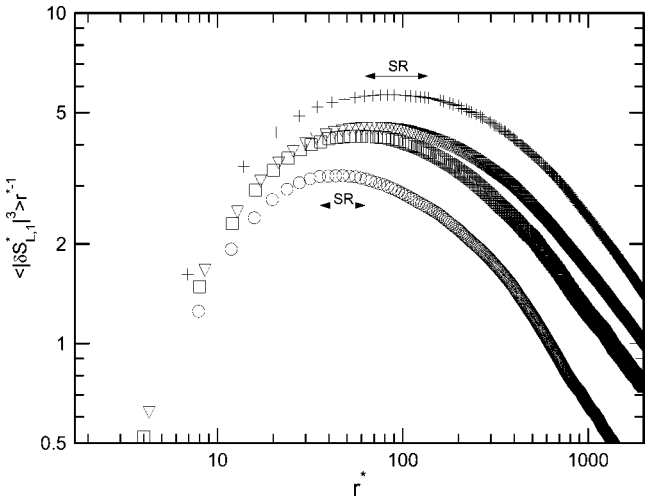

FIG. 3. Kolmogorov normalized third-order longitudinal structure functions multiplied by r^{*-1}: ○, $R_\lambda=100$; □, 200; ▽, 250; +, 300. The arrowed solid lines indicate the extent of the scaling range (SR).

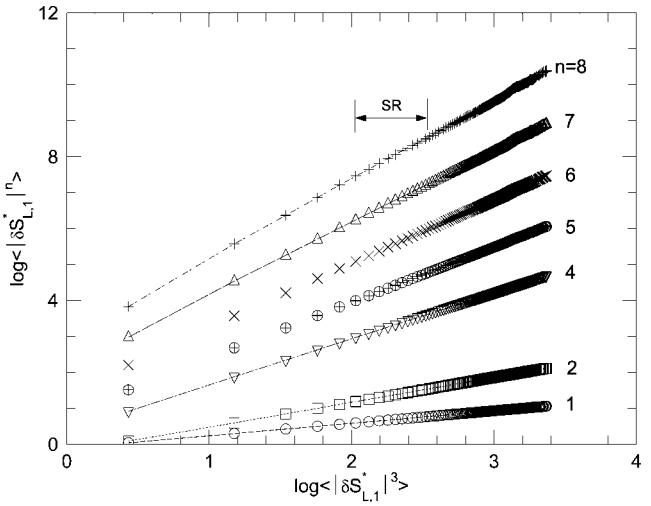

FIG. 4. Moments of order n (1–8) of $\langle|\delta S^*_{L,1}|^n\rangle$ as a function of $\langle|\delta S^*_{L,1}|^3\rangle$ ($R_\lambda=250$). The arrowed solid line indicates the extent of the scaling range (SR).

ranges for all the four values of R_λ. The peak value and width of the scaling range increase with R_λ. All the scaling exponents are estimated over the scaling range marked in Fig. 3 by using the ESS method. By plotting the nth-order velocity increments against the third-order moment of $|\delta S_L|$—i.e., $\langle|\delta S_L|^n\rangle\sim\langle|\delta S_L|^3\rangle^{\zeta_L(n)}$—the longitudinal scaling exponents can be estimated. Several methods have been used for estimating $\zeta_T(n)$ using variants of the ESS method. Dhruva *et al.* [24] and Antonia and Pearson [33] defined $\zeta_T(n)$ relative to the third-order moment of $|\delta S_L|$: i.e., $\langle|\delta S_{T,1}|^n\rangle\sim\langle|\delta S_L|^3\rangle^{\zeta_{T,1}(n)}$. There is evidence (e.g., [13,16,24]) to show that the magnitude of $\zeta_{T,1}(n)$ increases with R_λ and asymptotically approaches that of $\zeta_L(n)$ at large R_λ. Also, $\zeta_T(n)$ can be defined relative to the third-order moment of $|\delta S_T|$: i.e., $\langle|\delta S_{T,2}|^n\rangle\sim\langle|\delta S_{T,2}|^3\rangle^{\zeta_{T,2}(n)}$.

The longitudinal scaling exponents $\zeta_L(n)$ are obtained based on the following relation:

$$\langle|\delta S^*_{L,1}|^n\rangle\sim\langle|\delta S^*_{L,1}|^3\rangle^{\zeta_{L,1}(n)}. \tag{9}$$

From the plot of $\log\langle|\delta S^*_{L,1}|^n\rangle\sim\log\langle|\delta S^*_{L,1}|^3\rangle$ at $R_\lambda=250$ (Fig. 4) (distributions of $\log\langle|\delta S^*_{L,1}|^n\rangle$ vs $\log\langle|\delta S^*_{L,1}|^3\rangle$ for other values of R_λ are not shown here), scaling exponents $\zeta_{L,1}(n)$ were estimated from the least-squares linear regressions over the scaling range obtained from Fig. 3. It can be seen that the experimental data show excellent linearity over a range which is much wider than that shown in Fig. 3 for $R_\lambda=250$.

The scaling exponents of the nth-order moments of the longitudinal increments for different values of R_λ are shown in Fig. 5(a). It can be seen that the scaling exponents $\zeta_{L,1}(n)$ do not depend on R_λ. The very small difference of $\zeta_{L,1}(n)$ between different R_λ may be due to the limited sampling points in the present experiments. The values of $\zeta_{L,1}(n)$ depart significantly from the prediction of K41 (i.e., $n/3$) for $n>4$. This may indicate the increased effect of the intermittency for higher orders of the longitudinal velocity increments. The predictions of $\zeta_L(n)$ using the lognormal model (K62) and the She-Leveque (SL) model [34] are also shown for comparison in Fig. 5(a). For K62,

$$\zeta_L(n)=\frac{n}{3}-\frac{\mu}{18}n(n-3), \tag{10}$$

where μ is the intermittency parameter with a magnitude of 0.2–0.3. The value of μ can be obtained using the sixth-order velocity structure function since $\langle(\delta S_L)^6\rangle\sim r^{2-\mu}$ [i.e., $\mu=2-\zeta_{L,1}(6)$] in the inertial range. For the She-Leveque [34] model,

$$\zeta_u(n)=\frac{n}{9}+2\left[1-\left(\frac{2}{3}\right)^{n/3}\right]. \tag{11}$$

The measured values of $\zeta_{L,1}(n)$ show satisfactory agreement with that predicted by K62 and the SL model.

Another way to estimate the scaling exponents of the longitudinal velocity increments can be represented by Eq. (12), where w is the velocity component in the spanwise (z) direction. The scaling exponents can then be obtained from the plot of

$$\log\langle|\delta S^*_{L,2}|^n\rangle\sim\log\langle|\delta S^*_{L,2}|^3\rangle^{\zeta_{L,2}(n)}. \tag{12}$$

The scaling range over which $\log\langle|\delta S^*_{L,2}|^n\rangle$ depends linearly on $\log\langle|\delta S^*_{L,2}|^3\rangle$ is well defined (figure is not shown here). The scaling exponents defined by Eq. (12) are shown in Fig. 5(b). They agree satisfactorily with the predictions of K62 and the SL model. The present results (Fig. 5) seem to suggest that the scaling exponents of both spatial and temporal longitudinal velocity increments agree well with the predictions of K62 and SL.

The scaling exponents of the transverse velocity increments are also estimated using the ESS method over the same scaling range as for the longitudinal ones (Fig. 3). As there are a few methods to define the transverse velocity increments, the scaling exponents can be obtained as follows:

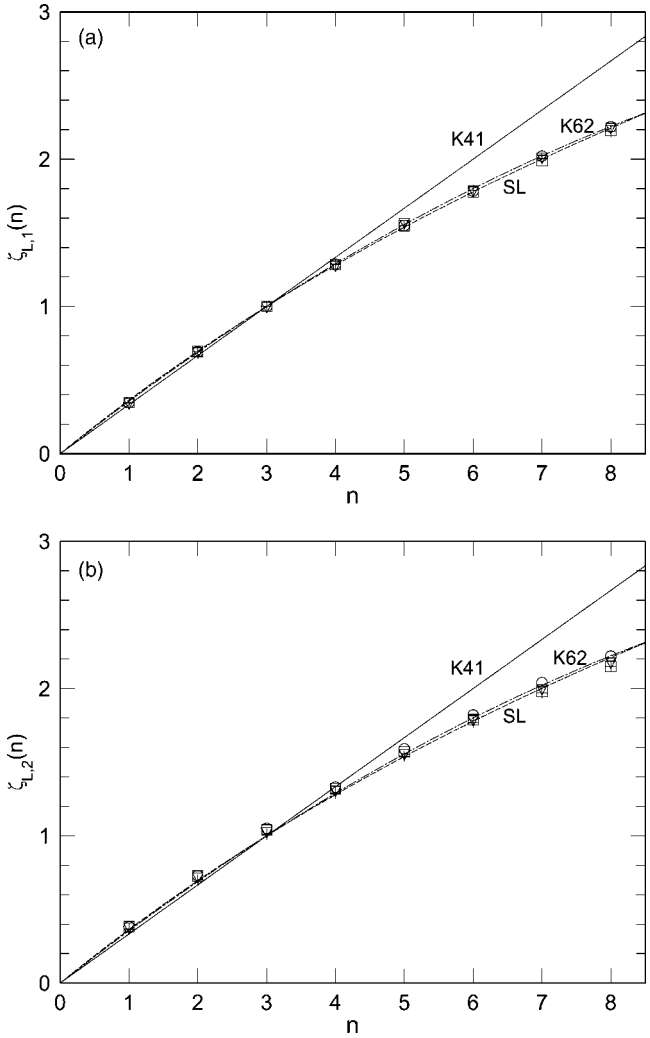

FIG. 5. Scaling exponents $\zeta_L(n)$ as a function of n at different R_λ: ○, $R_\lambda=100$; □, 200; ▽, 250; +, 300; △, $\zeta_{L,1}(n)$ ($R_\lambda=250$); solid line, K41 [1]; dot-dashed line, K62 [2]; dashed line, SL [34]. (a) $\zeta_{L,1}(n)$ and (b) $\zeta_{L,2}(n)$.

$$\langle|\delta S_{T,1}|^n\rangle \sim \langle|\delta S_{L,1}|^3\rangle^{\zeta_{T,1}(n)}, \tag{13}$$

$$\langle|\delta S_{T,2}|^n\rangle \sim \langle|\delta S_{L,2}|^3\rangle^{\zeta_{T,2}(n)}. \tag{14}$$

The transverse scaling exponents $\zeta_{T,1}(n)$ obtained from Eq. (13) for the four different Reynolds numbers in the present study are shown in Fig. 6. The longitudinal scaling exponents $\zeta_{L,1}(n)$ and the predictions using K62 with $\mu=0.2$ and the K41 and SL models are also shown for comparison. Obviously, $\zeta_{T,1}(n)$ are much smaller than $\zeta_{L,1}(n)$ for all orders, independent of R_λ. It seems that with the increase of R_λ, $\zeta_{T,1}(n)$ also increases, especially for high orders, indicating a weak dependence of $\zeta_{T,1}(n)$ on R_λ. This result is in consistence with that reported by Antonia *et al.* [13] and Zhou and Antonia [15]. It is conjectured that the difference between $\zeta_{T,1}(n)$ and $\zeta_{L,1}(n)$ may diminish when R_λ goes to infinity because the separation between the integral length scale and the inertial range scales increases with R_λ, thus reducing the influence from the large-scale anisotropy [16]. Another reason for the difference between $\zeta_{T,1}(n)$ and $\zeta_{L,1}(n)$ may be due to the global anisotropy of the flow field, as revealed by the ratio w'/u' ($\cong 0.85$ in the present wake flows). The effect of large-scale anisotropy on the scaling exponents can be examined by using the following definition [16]:

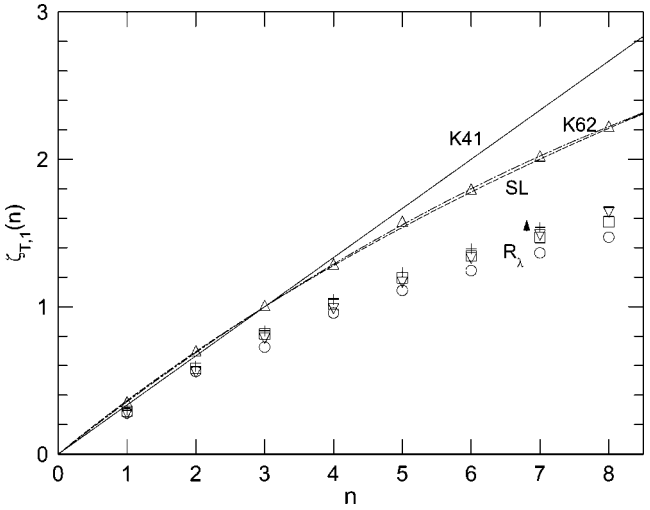

FIG. 6. Scaling exponents $\zeta_{T,1}(n)$ as a function of n at different R_λ: ○, $R_\lambda=100$; □, 200; ▽, 250; +, 300; △, $\zeta_{L,1}(n)$ ($R_\lambda=250$); solid line, K41 [1]; dot-dashed line, K62 [2]; dashed line, SL [34].

$$\psi_{uw}(n,r^*) = d\log\langle(\delta S^*_{T,1})^n\rangle/d\log\langle((\delta S^*_L)^n)\rangle. \tag{15}$$

If the two structure functions $\langle(\delta S^*_{T,1})^n\rangle$ and $\langle(\delta S^*_L)^n\rangle$ scale in similar manner over the same region of r^*, then $\psi_{uw}(n,r^*)=1$. Figure 7 shows the local relative scaling between $\langle(\delta S^*_{T,1})^n\rangle$ and $\langle(\delta S^*_L)^n\rangle$ for the case of $n=2$ at different Reynolds numbers. $\psi_{uw}(2,r^*)$ is close to 1 only for $r^*\leqslant 8$ (i.e., in the dissipative region). The maximum deviation (10%–20%) from 1 of $\psi_{uw}(2,r^*)$ occurs over the region of $r^*=8-40$,

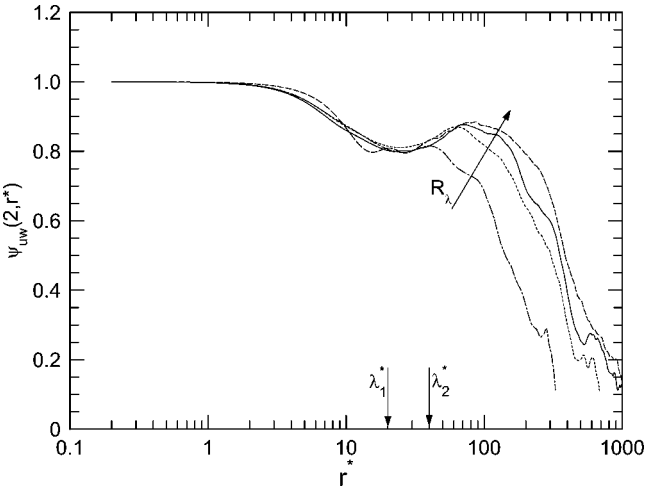

FIG. 7. Dependence of the relative local scaling exponents $\psi_{uw}(2,r^*)$ on r^* at various R_λ: dot-dashed line, $R_\lambda=100$; short-dashed line, 200; solid line, 250; long-dashed line, 300. λ_1^* and λ_2^* are the Taylor microscales normalized by η for $R_\lambda=100$ and 300, respectively. The arrow indicates the direction of increasing R_λ.

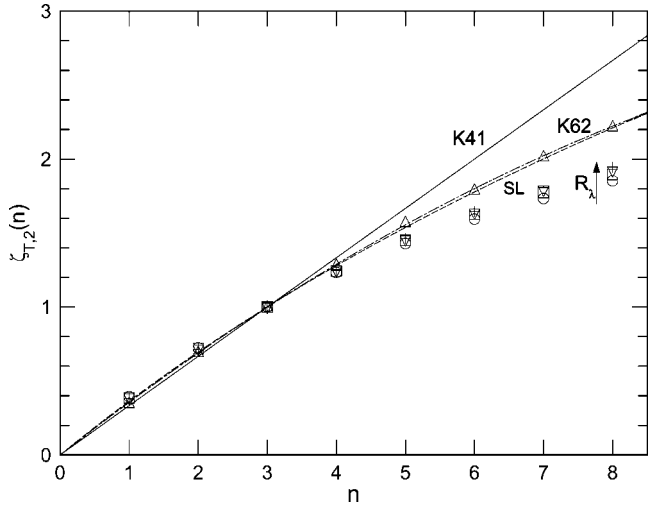

FIG. 8. Scaling exponents $\zeta_{T,2}(n)$ as a function of n at different R_λ: ○, $R_\lambda=100$; □, 200; ▽, 250; +, 300; △, $\zeta_{L,1}(n)$ ($R_\lambda=250$); solid line, K41 [1]; dot-dashed-line, K62 [2]; dashed line, SL [34].

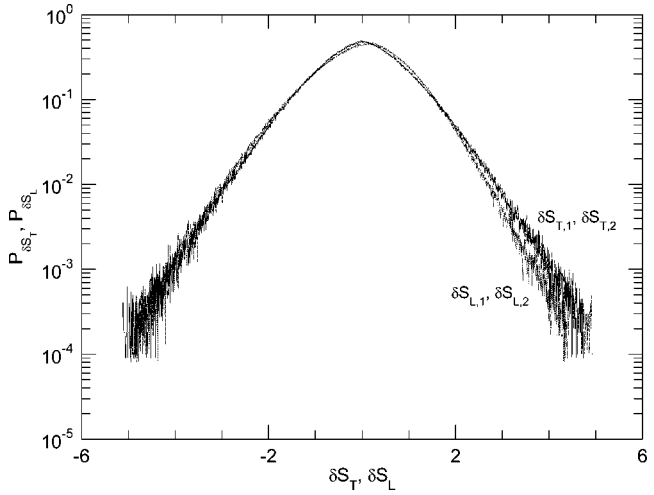

FIG. 9. PDF's of the velocity increments for inertial range separation $r^*=38$ at $R_\lambda=250$: dot-dashed line, $\delta S_{L,1}$; short-dashed line, $\delta S_{L,2}$; solid line, $\delta S_{T,1}$; long-dashed line, $\delta S_{T,2}$.

which corresponds to the Taylor microscale λ^*. The behavior of $\psi_{uw}(2,r^*)$ in the region of $r^*=8-40$ indicates that the large-scale anisotropy can "penetrate" into the inertial range scales, resulting in a departure in the scaling exponents of $\langle(\delta S^*_{T,1})^n\rangle$ from that of $\langle(\delta S^*_L)^n\rangle$. It is expected that with the further increase of R_λ, the deviation of $\psi_{uw}(2,r^*)$ from 1 in the scaling range will be reduced. This trend is in accordance with the results reported by Pearson and Antonia [16] for the jets and atmospheric surface layer data at much higher R_λ (=500–4250). The significant departure of $\psi_{uw}(2,r^*)$ from 1 for $r^*>100$ represents the influence of the large-scale anisotropy.

The scaling exponents $\zeta_{T,2}(n)$ obtained using Eq. (14) are shown in Fig. 8. They agree favorably with $\zeta_{L,1}(n)$ and the K62 and SL models for $n\leqslant 4$. When $n\geqslant 5$, the departure of $\zeta_{T,2}(n)$ from the above two model predictions is apparent. The magnitude of $\zeta_{T,2}(n)$ also reveals a weak dependence on R_λ; with the increase in R_λ, $\zeta_{T,2}(n)$ increases slowly. The difference between $\zeta_{L,1}(n)$ and $\zeta_{T,2}(n)$ as shown in Fig. 8 is smaller than that between $\zeta_{L,1}(n)$ and $\zeta_{T,1}(n)$ (Fig. 6). The difference between $\zeta_{L,1}(n)$ [or $\zeta_{L,2}(n)$] and $\zeta_{T,1}(n)$ [or $\zeta_{T,2}(n)$] may reflect the different intermittency of the velocity increments. This can be illustrated by the probability density function (PDF) of the velocity increments as shown in Fig. 9, where the PDF of the longitudinal and transverse velocity increments for separation $r^*=38$ in the scaling range are plotted and compared. Clearly, the distributions of the PDF's of $\delta S_{T,1}$ and $\delta S_{T,2}$ are more stretched for large fluctuations than that of $\delta S_{L,1}$ and $\delta S_{L,2}$, indicating the stronger intermittency of the former than the latter.

V. REFINED SIMILARITY HYPOTHESIS FOR TRANSVERSE VELOCITY INCREMENTS

Boratav and Pelz [14] suggested that the inequality mainly reflects the greater contribution to intermittency from the enstrophy-dominated structures than from the strain-dominated structures. Chen *et al.* [11] proposed a modification to the RSH (K62) for the transverse velocity increments, which they called the RSHT. For the RSHT, it is assumed that the transverse velocity increments are associated with the locally averaged enstrophy whereas the longitudinal velocity increments are associated with the locally averaged energy dissipation rate:

$$\langle(\delta S_L)^n\rangle \sim D_L^n\langle\varepsilon_r^{n/3}\rangle r^{n/3} \quad \text{(RSH)}, \tag{16}$$

$$\langle(\delta S_T)^n\rangle \sim D_T^n\langle\Omega_r^{n/3}\rangle r^{n/3} \quad \text{(RSHT)}, \tag{17}$$

where D_L^n and D_T^n are constants, and Ω_r [$\Omega\equiv\nu(\omega_x^2+\omega_y^2+\omega_z^2)$] and ε_r are the locally averaged enstrophy and energy dissipation rate, respectively, which are obtained using

$$\varepsilon_r=\frac{1}{r}\int_{x_0-r/2}^{x_0+r/2}\varepsilon(r)dx, \tag{18}$$

$$\Omega_r=\frac{1}{r}\int_{x_0-r/2}^{x_0+r/2}\Omega(r)dx, \tag{19}$$

where the spatial integration on x is converted from the temporal one by applying Taylor's hypothesis. It is assumed that $\langle\varepsilon_r^n\rangle$ and $\langle\Omega_r^n\rangle$ scale as $r^{\tau^d(n)}$ and $r^{\tau^o(n)}$, respectively. Therefore, in the RSH and RSHT, the scaling of the longitudinal and transverse velocity increments can be expressed as

$$\zeta_L(n)=\frac{n}{3}+\tau^d(n/3), \tag{20}$$

$$\zeta_T(n)=\frac{n}{3}+\tau^o(n/3). \tag{21}$$

If the RSH and RSHT work satisfactorily, $\tau^d(n/3)$ and $\tau^o(n/3)$ should be both negative and the magnitudes of $\zeta_L(n)-\tau^d(n/3)$ and $\zeta_T(n)-\tau^o(n/3)$ should be equal to $n/3$.

In the present study, the longitudinal and spanwise velocity components u and w are measured using two X-wire

TABLE I. Scaling exponents of locally averaged energy dissipation rate and enstrophy at various R_λ.

R_λ	100		200		250		300	
n	$\tau^o(n/3)$	$\tau^d(n/3)$	$\tau^o(n/3)$	$\tau^d(n/3)$	$\tau^o(n/3)$	$\tau^d(n/3)$	$\tau^o(n/3)$	$\tau^d(n/3)$
1	0.0488 (±0.0016)	0.0193 (±0.0013)	0.052 (±0.0018)	0.0226 (±0.0015)	0.101 (±0.0068)	0.014 (±0.0006)	0.064 (±0.0038)	0.04 (±0.0043)
2	0.0388 (±0.0016)	0.1412 (±0.0017)	0.037 (±0.0017)	0.0135 (±0.0018)	0.05 (±0.0066)	0.01 (±0.0008)	0.037 (±0.0038)	0.018 (±0.0051)
3	−0.0125 (±0.0012)	−0.0134 (±0.002)	−0.0156 (±0.0014)	−0.0161 (±0.0022)	−0.0174 (±0.0064)	−0.016 (±0.0001)	−0.0138 (±0.0038)	−0.016 (±0.006)
4	−0.102 (±0.0013)	−0.063 (±0.0024)	−0.103 (±0.0015)	−0.0665 (±0.0025)	−0.107 (±0.0061)	−0.063 (±0.001)	−0.09 (±0.004)	−0.063 (±0.0064)
5	−0.226 (±0.0016)	−0.134 (±0.0026)	−0.223 (±0.0016)	−0.137 (±0.0027)	−0.22 (±0.0056)	−0.13 (±0.001)	−0.192 (±0.0042)	−0.127 (±0.0068)
6	−0.383 (±0.0018)	−0.227 (±0.0028)	−0.371 (±0.0017)	−0.228 (±0.0029)	−0.356 (±0.0053)	−0.216 (±0.0011)	−0.318 (±0.0044)	−0.213 (±0.007)
7	−0.569 (±0.0022)	−0.34 (±0.003)	−0.545 (±0.0019)	−0.337 (±0.0031)	−0.517 (±0.0055)	−0.321 (±0.0012)	−0.47 (±0.0046)	−0.342 (±0.007)
8	−0.781 (±0.0025)	−0.457 (±0.0032)	−0.74 (±0.002)	−0.464 (±0.0032)	−0.7 (±0.0058)	−0.445 (±0.0014)	−0.645 (±0.0047)	−0.555 (±0.0065)

probes (Fig. 1). Three velocity gradients—i.e., $\partial u/\partial x$, $\partial u/\partial z$, and $\partial w/\partial x$—are measured simultaneously. The energy dissipation rate ε can then be approximated using the relation [35]

$$\varepsilon_{\mathrm{ap}} = \nu[6(\partial u/\partial x)^2 + 3(\partial u/\partial z)^2 + 2(\partial w/\partial x)^2 + 2(\partial u/\partial z) \times (\partial w/\partial x)]. \quad (22)$$

This relation has been verified in grid turbulence to be more reliable than the isotropic relation—i.e., $\varepsilon_{\mathrm{iso}}=15\nu(\partial u/\partial x)^2$. Even though only the transverse vorticity component is measured using the two X-wire probes [Eq. (7)], by assuming local isotropy, the enstrophy can be approximated by

$$\Omega = 3\nu\omega_y^2. \quad (23)$$

The scaling exponents $\tau^d(n/3)$ and $\tau^o(n/3)$ are inferred from the distributions of $\log\langle\varepsilon_r^{n/3}\rangle$ and $\log\langle\Omega_r^{n/3}\rangle$ over the same scaling range of r^* as that used to estimate $\zeta_{L,1}(n)$ and $\zeta_{T,1}(n)$. The least-squares linear fits to the measured data are reliable with correlation coefficient being always larger than 0.98 over the scaling range. The values of $\tau^d(n/3)$ and $\tau^o(n/3)$ are listed in Table I for the four Reynolds numbers covered in the present study. The numbers inside the brackets represent the corresponding standard deviations of the fits. It can be seen that the values of $|\tau^o(n/3)|$ are always larger than that of $|\tau^d(n/3)|$, indicating that $\langle(\nu\Omega_r)^{n/3}\rangle$ is more intermittent than $\langle\varepsilon_r^{n/3}\rangle$. This result is consistent with that reported by Chen *et al.* [36] using DNS. The magnitudes of $\tau^d(n/3)$ keep approximately constant with the increase of R_λ, resulting in constant values of $\zeta_L(n)$ at different R_λ. This result is consistent with that shown in Fig. 5. In contrast, the magnitudes of $|\tau^o(n/3)|$ decrease with the increase in R_λ, indicating a reduced intermittency effect in the scaling range with the increase in R_λ. It is conjectured that the scaling exponents of $\langle\varepsilon_r^{n/3}\rangle$ and $\langle(\nu\Omega_r)^{n/3}\rangle$ may be equivalent in the case when R_λ is extremely large. This trend is consistent with that reported by Nelkin [25,26]. However, this result does not necessary mean that at sufficiently high Reynolds numbers the flow will become globally isotropy. Anisotropy at large scales may still persist. For sufficiently high Reynolds numbers, as the separation between the integral length scales and the inertial range scales is large, the influence of the anisotropy effects will not dominate in the inertial range. The values of $\zeta_L(n)-\tau^d(n/3)$ and $\zeta_T(n)-\tau^o(n/3)$, with $\zeta_L(n)$ representing $\zeta_{L,1}(n)$ and $\zeta_{L,2}(n)$ and $\zeta_T(n)$ representing $\zeta_{T,1}(n)$ and $\zeta_{T,2}(n)$, respectively, are compared with $n/3$ in Figs. 10 and 11. There should be satisfactory agreements between $\zeta_L(n)-\tau^d(n/3)$ and $\zeta_T(n)-\tau^o(n/3)$ with $n/3$ if the RSH and RSHT work well. This is indeed the case for $\zeta_L(n)-\tau^d(n/3)$ [Fig. 10] with a deviation less than 3% both for the spatial and temporal longitudinal velocity increments. However, the agreement between $\zeta_T(n)-\tau^o(n/3)$ and $n/3$ depends on the definition of the transverse velocity increments (Fig. 11). Since there is satisfactory agreement (with deviation less than 3%) between $\zeta_{T,2}(n)-\tau^o(n/3)$ and $n/3$, independent of R_λ, this result indicates that the RSHT works well for the spatial transverse velocity increments to explain the departure of $\zeta_{T,2}(n)$ from $\zeta_L(n)$, supporting the experimental results of Bi and Wei [10]. It needs to be noted that the verification of the RSHT using $\zeta_{T,2}(n)$ [Fig. 11(b)] is based on the assumption that $\Omega=3\nu\omega_y^2$. However, the intermittency characteristics of the enstrophy Ω ($\equiv\nu\omega_i\omega_i$) may not be accurately represented by $3\nu\omega_y^2$. In this case, satisfactory agreement between $\zeta_{T,2}(n)-\tau^o(n/3)$ and $n/3$ may not be obtained. The discrepancy of the present results [Fig. 11(b)] from that reported by Antonia *et al.* [13] and Zhou and Antonia [15] is due to the different definitions of the transverse velocity increments, where only $\zeta_{T,1}(n)$ estimated from the temporal transverse velocity increments are reported. The departure of

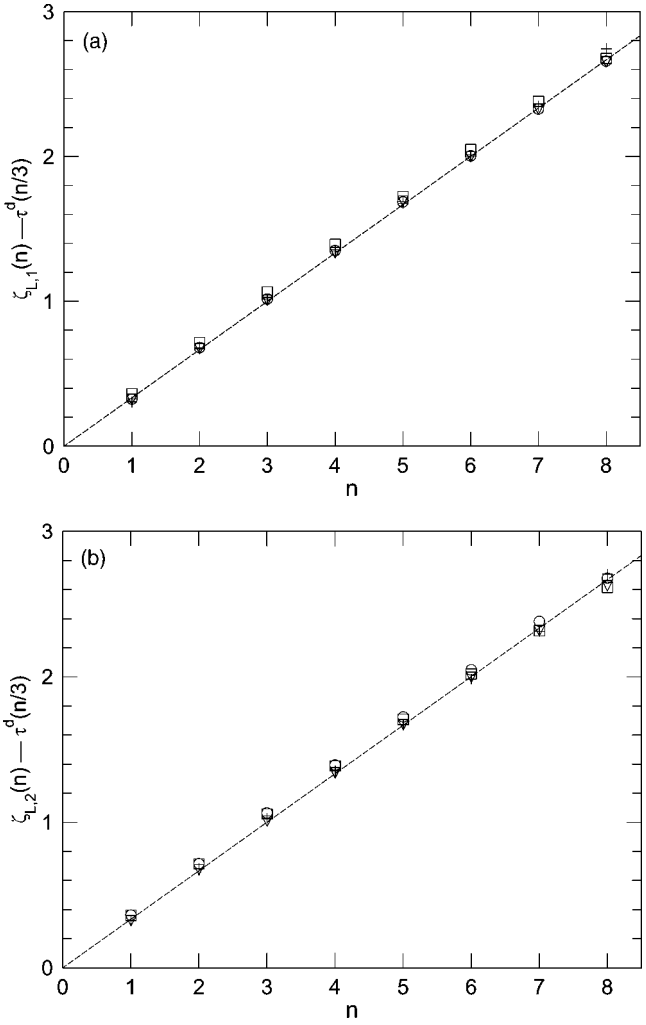

FIG. 10. Verification of RSH for the longitudinal scaling exponents at different R_λ: ○, $R_\lambda = 100$; □, 200; ▽, 250; +, 300. (a) $\zeta_{L,1}(n) - \tau^d(n/3)$ and (b) $\zeta_{L,2}(n) - \tau^d(n/3)$.

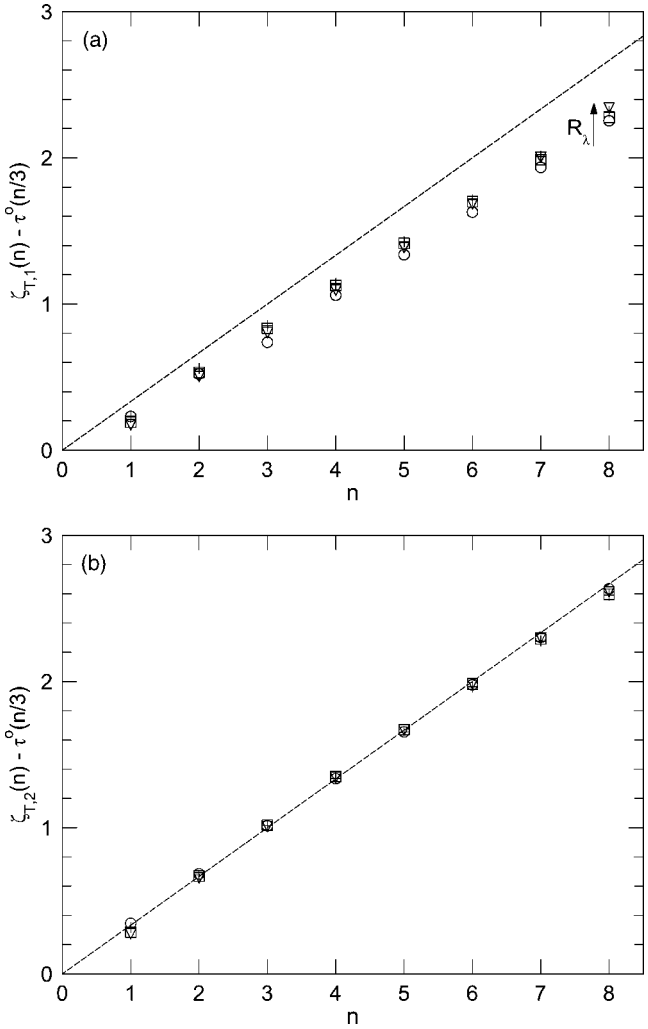

FIG. 11. Verification of the RSHT for the transverse scaling exponents at different R_λ: ○, $R_\lambda = 100$; □, 200; ▽, 250; +, 300. (a) $\zeta_{T,1}(n) - \tau^d(n/3)$ and (b) $\zeta_{T,2}(n) - \tau^d(n/3)$.

$\zeta_{T,1}(n) - \tau^o(n/3)$ from $n/3$ is still significant and cannot be attributed to the experimental uncertainty, even though there is a trend that $\zeta_{T,1}(n) - \tau^o(n/3)$ approaches $n/3$ slowly when R_λ increases. It seems that the RSHT can only partially account for the inequality between $\zeta_{T,1}(n)$ and $\zeta_{L,1}(n)$ or $\zeta_{L,2}(n)$, at least for the present low to moderate Reynolds numbers. Even though the present results are obtained at low and moderate Reynolds numbers, the dependence of the transverse scaling exponents on Reynolds number is consistent with that obtained over a much larger range of R_λ [16]. Therefore, we believe that at very high R_λ, the scaling of the longitudinal and transverse velocity increments should be the same. At low to moderate R_λ, the present results suggest that the scaling of the transverse velocity increments depends not only on R_λ, but also on the large-scale anisotropy.

VI. CONCLUSIONS

Longitudinal and transverse velocity increments are measured both temporally and spatially using two X-wire probes separated in the spanwise direction in the intermediate region of a cylinder wake over Taylor microscale Reynolds number of the range of 100–300. The two X-wire probes also allow measurements of the transverse vorticity component when the separation is small enough. The scaling exponents of the longitudinal velocity increments for both temporal and spatial measurements agree favorably with the predictions of K62 and the SL model. The scaling exponents of the transverse velocity increments are considerably smaller than those of the longitudinal ones, with the values for spatial transverse increments being slightly larger than the temporal ones. Both of them increase slowly with R_λ. The association of the scaling of the longitudinal and transverse velocity increments with the locally averaged energy dissipation rate (RSH) and enstrophy (RSHT) are also examined. While the scaling exponents of the locally averaged dissipation rate does not depend on R_λ, the scaling exponents of the locally averaged enstrophy decrease with R_λ, a trend that is consistent with that reported by Nelkin [25,26]. The present results

show that the RSH works satisfactorily for longitudinal velocity increments. The RSHT can account for the difference between the scaling exponents of the longitudinal and spatial transverse velocity increments, but can account for only partially the different scalings between the longitudinal and temporal transverse velocity increments. A more likely source for the latter difference is the large-scale anisotropy of the velocity field at low and moderate R_λ.

[1] A. N. Kolmogorov, C. R. Acad. Sci. SSSR **30**, 301 (1941).
[2] A. N. Kolmogorov, J. Fluid Mech. **13**, 82 (1962).
[3] H. Kahalerras, H. Malecot, and Y. Gagne, in *Advances in Turbulence VI*, edited by S. Gavrilakis, L. Machiels, and P. A. Monkewitz (Kluwer Academic, Dordrecht, 1996), p. 235.
[4] R. Camussi, D. Barbagallo, G. Guj, and F. Stella, Phys. Fluids **8**, 1181 (1996).
[5] A. Noullez, G. Wallace, W. Lempert, R. B. Miles, and U. Frisch, J. Fluid Mech. **339**, 287 (1997).
[6] R. Camussi and R. Benzi, Phys. Fluids **9**, 257 (1997).
[7] W. van de Water and J. A. Herweijer, J. Fluid Mech. **387**, 3 (1999).
[8] T. Zhou, B. R. Pearson, and R. A. Antonia, Fluid Dyn. Res. **28**, 127 (2001).
[9] R. A. Antonia, T. Zhou, and G. P. Romano, J. Fluid Mech. **459**, 67 (2002).
[10] W. Bi and Q. Wei, J. Turbul. **4**, 28 (2003).
[11] S. Y. Chen, K. R. Sreenivasan, M. Nelkin, and N. Cao, Phys. Rev. Lett. **79**, 1253 (1997).
[12] S. Grossman, D. Lohse, and A. Reeh, Phys. Fluids **9**, 3817 (1997).
[13] R. A. Antonia, T. Zhou, and Y. Zhu, J. Fluid Mech. **374**, 29 (1998).
[14] O. N. Boratav and R. B. Pelz, Phys. Fluids **9**, 1400 (1997).
[15] T. Zhou and R. A. Antonia, J. Fluid Mech. **406**, 81 (2000).
[16] B. R. Pearson and R. A. Antonia, J. Fluid Mech. **444**, 343 (2001).
[17] I. Arad, B. Dhruva, S. Kurien, V. L'vov, I. Procaccia, and K. R. Sreenivasan, Phys. Rev. Lett. **81**, 5330 (1998).
[18] I. Arad, V. L'vov, and I. Procaccia, Phys. Rev. E **59**, 6753 (1999).
[19] I. Arad, L. Biferale, I. Mazzitelli, and I. Procaccia, Phys. Rev. Lett. **82**, 5040 (1999).
[20] S. Kurien and K. R. Sreenivasan, Phys. Rev. E **62**, 2206 (2000).
[21] L. Beferale and M. Vergassola, Phys. Fluids **13**, 2139 (2001).
[22] L. Biferale and F. Toschi, Phys. Rev. Lett. **86**, 4831 (2001).
[23] G. P. Romano and R. A. Antonia, J. Fluid Mech. **436**, 231 (2001).
[24] B. Dhruva, Y. Tsuji, and K. R. Sreenivasan, Phys. Rev. E **56**, R4928 (1997).
[25] M. Nelkin, Phys. Fluids **11**, 2202 (1999).
[26] M. Nelkin, Am. J. Phys. **68**, 310 (2000).
[27] R. A. Antonia, B. R. Pearson, and T. Zhou, Phys. Fluids **12**, 3000 (2000).
[28] R. A. Antonia and B. R. Pearson, Phys. Rev. E **62**, 8086 (2000).
[29] V. L'vov and I. Procaccia, Phys. Fluids **8**, 2565 (1996).
[30] A. S. Monin and A. M. Yaglom, *Statistical Fluid Mechanics* (MIT Press, Cambridge, MA, 1975), Vol. 2.
[31] R. Benzi, S. Ciliberto, R. Tripiccione, C. Baudet, F. Massaioli, and S. Succi, Phys. Rev. E **48**, R29 (1993).
[32] G. Stolovitzky and K. R. Sreenivasan, Phys. Rev. E **48**, R33 (1993).
[33] R. A. Antonia and B. R. Pearson, Europhys. Lett. **40**, 393 (1997).
[34] Z. S. She and E. Leveque, Phys. Rev. Lett. **72**, 336 (1994).
[35] T. Zhou and R. A. Antonia, Phys. Fluids **12**, 335 (2000).
[36] S. Y. Chen, K. R. Sreenivasan, and M. Nelkin, Phys. Rev. Lett. **79**, 1253 (1997).